Arab J Sci Eng (2016) 41:1757–1769
DOI 10.1007/s13369-015-1889-1

RESEARCH ARTICLE - MECHANICAL ENGINEERING

Fabrication of In-Situ Al–Cu Intermetallics on Aluminum Surface by Friction Stir Processing

Essam R. I. Mahmoud[1,2] · **Ali M. A. Al-qozaim**[1]

Received: 6 June 2015 / Accepted: 6 October 2015 / Published online: 17 November 2015

Abstract In-situ Al–Cu intermetallic metal matrix composites (MMCs) surface layer has been fabricated on an A 1050-H24 aluminum plate by friction stir processing (FSP). Pure Cu powder of 5 μm in size was packed into a groove cut on the aluminum plate and covered with an aluminum sheet. A FSP tool of square probe shape, rotated at a rate of 750–1500 rpm, was plunged into the plate through the cover sheet and the groove and moved along the groove at traveling speed of 0.83 and 1.66 mm/s. Double and triple passes were applied. After the surface MMCs were fabricated on the Al plate, the type and homogeneity of the distributed particles inside the Al matrix have been evaluated from the macro-/microstructure and hardness distribution. As a result, it was found that the copper particles reacted with the aluminum matrix at almost all the processing conditions even during the first pass. Also, at a traveling speed of 1.66 mm/s, most of the resulted intermetallics were $CuAl_2$ at a rotation speed of 750 rpm, while the Cu-rich intermetallics (Al–Cu and Al_4Cu_9) appeared at rotation speeds of 1000 and 1500 rpm. Moreover, when the traveling speed was decreased to 0.83 mm/s, the amounts of the resulted intermetallics were increased. At a rotation and traveling speeds of 750 rpm and 0.83 mm/s, respectively, the nugget zone matrix consisted of nano-sized $CuAl_2$ intermetallics distributed in aluminum which increase the hardness to almost five times of the aluminum matrix adjacent to the nugget zone.

✉ Essam R. I. Mahmoud
emahoud@kku.edu.sa

[1] Mechanical Engineering, King Khalid University, Abha, Kingdom of Saudi Arabia

[2] Central Metallurgical Research and Development Institute (CMRDI), Cairo, Egypt

Keywords Friction stir processing · Aluminum · Copper powder · In-situ intermetallics · Surface composites

1 Introduction

Surface metal matrix composites (SMMCs) exhibit a unified combination of high tribological properties of the surface and high toughness of the interior bulk metal when compared to both metal matrix composites (MMCs) and monolithic materials. Selecting reinforcement remains one of the most critical factors in realizing the best properties from the resultant SMMCs [1,2]. On the other hand, it is widely recognized that the mechanical properties of metal matrix composites (MMCs) are controlled by the type, size and volume fraction of the reinforcement phase(s), and the nature of the matrix-reinforcement interface. Superior mechanical properties can be achieved when fine, thermally stable and hard reinforcement(s) with good and clean interfacial bonding are dispersed uniformly in the metal matrix. As suggested by several authors [3–5], such characteristics can be obtained when the reinforcements are formed inside the matrix during MMCs fabrication, i.e., in-situ intermetallics [3–5].

In-situ intermetallic compounds provide a new family of reinforcement phases ($CuAl_2$, $TiAl_3$, $FeAl_3$, etc.) which posses high specific strength, high specific modulus and excellent wear properties at both ambient and elevated temperatures. These reinforcements are formed in the matrix by reaction of the added element(s) with each other or with the matrix, so the resulted dispersed particles can be expected to be thermally stable and have strong interfacial bonding with the matrix [5–10]. Copper is one of the ideal elements to be added to aluminum for cladding applications due to its low cost and high wear resistance of the Al–Cu intermetallics [5,6]. It was reported by Dubourg et al. [5,6] that the Al–Cu intermetallic layer was fabricated by pre-placing the copper

powder on the aluminum surface and then heated beyond the melting point of the substrate by high-energy laser beam. The resulted surface layer showed high hardness and good wear resistance [5,6]. It must be pointed out, however, that the high-temperature surfacing techniques are often accompanied with fusion and solidification of the surface layer which causes some metallurgical defects such as porosity, clustering and hot cracks. Furthermore, the refining effect of the dispersed particles and the matrix microstructure is limited [11–14]. Considering these problems, friction stir processing (FSP) seems to be a good candidate for successful fabrication of intermetallics—SMMCs on the Al plate [1].

Friction stir processing (FSP) is a microstructure modification technique developed by Mishra and Mahoney [15] based on the concept of friction stir welding, but its goal is different [15,16]. A non-consumable rotating tool consisting of a shoulder and a probe is plunged into a single piece of material and provides frictional heating and mechanical mixing in the area covered by the tool [1,15]. It is considered that SMMCs are one of the latest applications of FSP [16,17]. The stirring action and frictional heat generated by the FSP tool can be used to distribute the hard particles as reinforcement on the surface of light metals like aluminum and magnesium [16,17].

Recently, some researchers [18–21] reported the successful fabrication of in-situ intermetallic-reinforced aluminum matrix from elemental powder mixtures of Al–Cu, Al–Ti and Al–Fe by FSP. That is, billets of powder mixtures were firstly prepared by the use of conventional press and sinter route. The sintered billets were then subjected to multiple passes of FSP until the reaction between the powders mixture completed. For example, Hsu et al. [18–20] detected the formation of $CuAl_2$ intermetallic compound from the powder mixture of Al–Cu and the Al_3Ti intermetallic compound from the powder mixture of Al–Ti.

In this work, we will present the feasibility to fabricate a thick layer of Al–Cu intermetallic SMMCs in the order of millimeters on aluminum alloy surface by taking advantages of particles dispersion, heat generation and stirring effect of the FSP.

2 Experimental Work

Commercially pure aluminum Al-1050-H24 plates of 5 mm thickness were used as the base material. A tool of steel SKD61 with a shoulder of 14 mm diameter and a square probe of 5 mm diagonal length and 3.3 mm height was used to perform the FSP. The average particle diameter of the pure copper powder used as reinforcement was 5 μm as shown in Fig. 1. The copper powders were packed in a groove of 3 mm width and 1.5 mm depth cut on the Al plate. The tool was rotated at a rate ranging from 750 to 1500 rpm and traveled at a speed of 0.83 and 1.66 mm/s with a tilt angle of 3°. Double and triple passes were applied in order to improve the homogeneity of the reinforcement particle distribution. In the second pass, the tool was traveled along the same line as the first and third ones but in the opposite direction. This means that the advancing side of the first and third passes became the retreating side in the second pass. Macro- and microstructure observations were performed on the cross section of the FSP specimens. Scanning electron microscope (SEM, ELIONIX, ERA-8800FE) was used to study the distribution of reinforcement particles. The microhardness was measured with AKASHI Model Vickers hardness tester at 200 g load applied for 15 s through the mid-plane of the cross section of the nugget of each condition. The hardness distribution was measured along three parallel lines that were 1–2 mm deep from the upper surface and separated by a distance of 0.5 mm. The interval between the indentations on the same line was 0.75 mm. All measured data along the three lines were collected and averaged for each condition. The nugget zones produced by FSP triple passes were analyzed by X-ray diffractometer (XRD, D 8 Discover with GADDS system, 35 kv, 80 mA, MoKα radiation) to identify experimentally the phases that were present inside the FSP nugget zone. Three point bending test was carried out at room temperatures under a bending angle of 90° for the face and side of the FSP nugget zone fabricated at a rotation speed of 750 rpm and traveling speeds of 0.83 and 1.66 mm/s, to check the ductility of the formed surface layer.

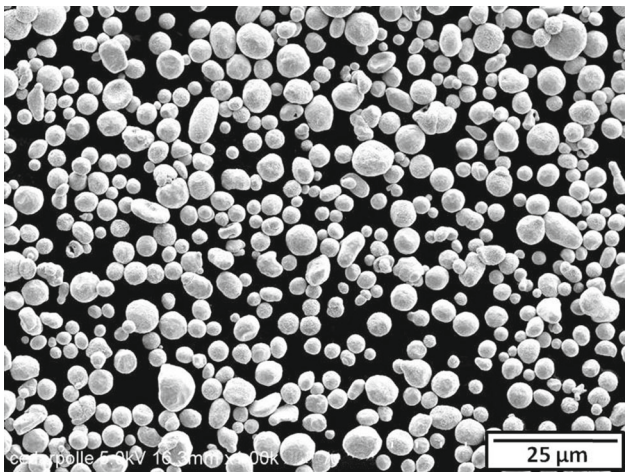

Fig. 1 SEM micrograph of as-received Cu powder

3 Results and Discussion

3.1 Surface Layer Properties After First Pass

Macroscopic appearances of the cross sections of the nugget zones produced by the first pass at a traveling speed of

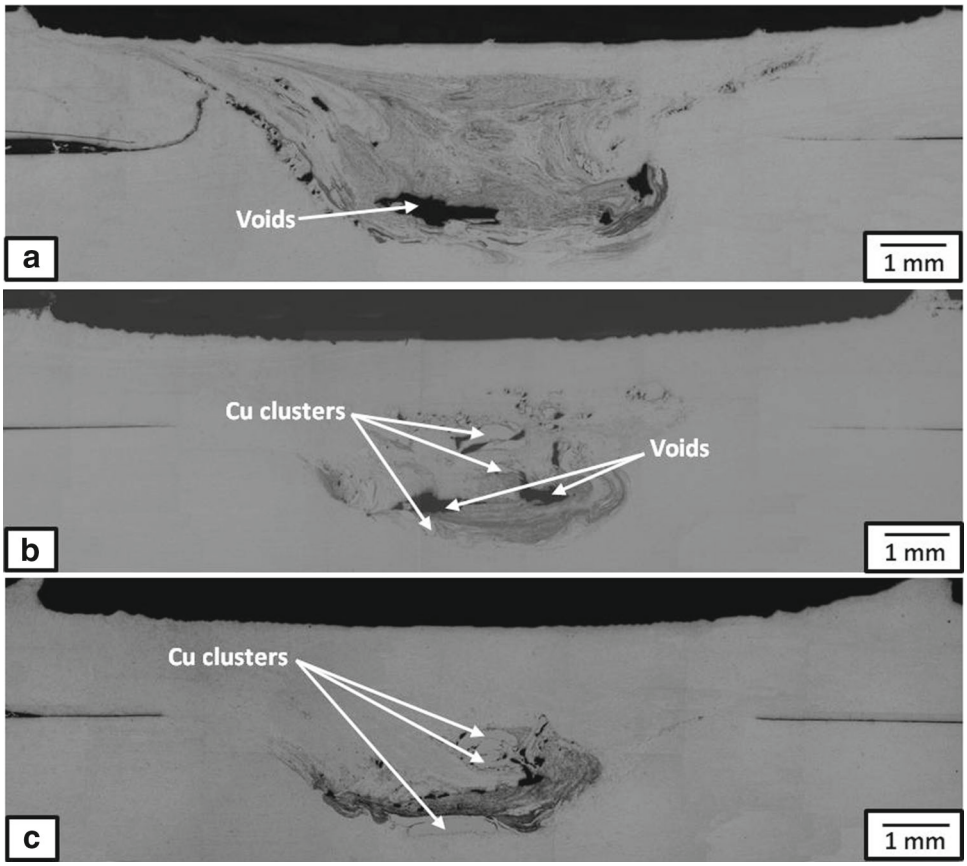

Fig. 2 Macrographs of the nugget zone cross sections produced by FSP first pass at a traveling speed of 1.66 mm/s and following rotation speeds: **a** 750 rpm, **b** 1000 rpm and **c** 1500 rpm. (Advancing side in the left side)

1.66 mm/s and rotation speeds of 750–1500 rpm are shown in Fig. 2. Firstly, the nugget zone in this stage consisted of four different microstructures: (1) areas (gray color) where some fine Cu/intermetallic particles were dispersed, (2) areas (brighter) where almost no dispersed particles were observed, (3) copper clusters (shown by arrows) and (4) voids (black color). The distributions of the dispersed particles within the nugget zone tended to be improved by decreasing the rotation speed. At a rotation speed of 750 rpm, the dispersed particles were distributed over most areas of the nugget zone, though some large voids were observed in the nugget zone bottom, while they tended to concentrate in the center of the nugget zone at a rotation speed of 1000 rpm. When the rotation speed was increased to 1500 rpm, the dispersed particles were distributed in a "C" shape area in the center of the nugget zone, leaving the rest of the nugget zone at much lower dispersed particles density. Some large Cu clusters were also observed when the rotation speeds were 1000 and 1500 rpm. The XRD patterns obtained from the nugget zone cross sections produced by the first FSP pass at a traveling speed of 1.66 mm/s are shown in Fig. 3. At all rotation speeds, the major peaks were identified as aluminum and copper. In addition to these, small diffraction peaks of $CuAl_2$ intermetallic phase were detected, which proved that the Cu particles reacted with the Al matrix during the first pass at rotation speeds not less than 750 rpm. Very small diffraction peaks of Al–Cu and Al_4Cu_9 intermetallic phases were also detected at rotation speeds of 1000 and 1500 rpm, suggesting that the reaction of the Cu particle with the Al matrix was enhanced with the increase in the FSP heat input.

The microstructure of the nugget zones cross sections was observed with a scanning electron microscope as shown in Fig. 4. When the rotation speed was 1500 rpm, the Cu particles were agglomerated into large clusters in specific areas in the nugget zone, as observed in Fig. 4a. On the other hand, when the rotation speed was 750 rpm, most of the dispersed particles were distributed as smaller clusters as shown in Fig. 4b, or in banding structures toward the advancing side as shown in Fig. 4c. Close view of a dispersed Cu particle (see Fig. 4d) showed that the reaction between the Cu particles and the Al matrix occurred on the Cu particles peripheral edges.

3.2 Surface Layer Properties After Triple Passes

3.2.1 Macrostructure of the Nugget Zone

Macroscopic appearances of the nuggets cross sections produced by triple FSP passes at rotation speeds of 750–1500 rpm and traveling speeds of 0.83 and 1.66 mm/s are

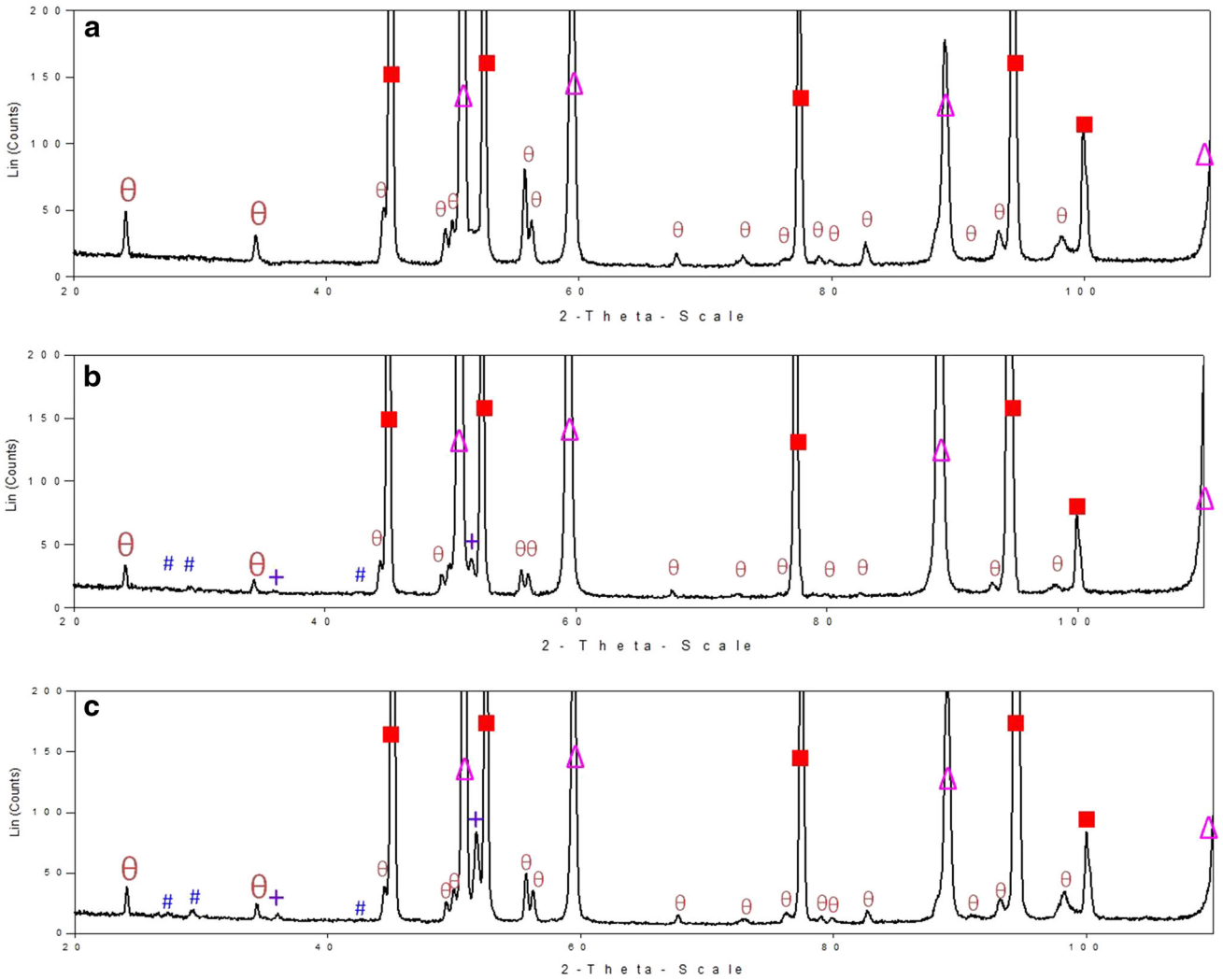

Fig. 3 XRD patterns obtained from nugget zone cross section at a traveling speed of 1.66 mm/s after first pass, where **a** rotation speed of 750 rpm, **b** rotation speed of 1000 rpm, and **c** rotation speed of 1500 rpm. (*filled square* Al, *triangle* Cu, *theta symbol* $CuAl_2$, *hash symbol* Al–Cu, *plus symbol* Al_4Cu_9)

shown in Fig. 5. The distribution of the dispersed particles was improved by the triple passes, since the stirring action generated in every pass by the rotated tool dispersed the particles more widely and uniformly in the nugget zone. It can be also seen from this figure that the dispersed particles were distributed more homogenously by decreasing the rotation speed. At a rotation speed of 750 rpm, the dispersed particles were distributed over almost whole area of the nugget zone without any cracks or any other macroscopic defects. The dispersed particles density was slightly increased with the depth from the nugget surface. On the other hand, the use of rotation speed more than 750 rpm resulted in inhomogeneous distribution of the dispersed particles; the particles tended to concentrate at the bottom of the nugget zone. Moreover, as indicated by arrows in Fig. 5c–f, some large voids remained at the bottom of the nugget zone in addition to large Cu clusters. On the other hand, the traveling speed had a minor effect on the macroscale behavior of the material inside the nugget zone, comparing with the effect of rotation speed.

3.2.2 Microstructure of the Nugget Zone

The X-ray diffraction (XRD) patterns obtained from the cross sections of the nugget zone produced after triple passes at rotation speeds of 750–1500 rpm and traveling speeds of 0.83 and 1.66 mm/s are shown in Fig. 6. All of the observed nugget zones consisted of mixtures of Al, Cu, $CuAl_2$, Al–Cu and Al_4Cu_9 with different ratios. The large intensities of the Al peaks were mainly due to the matrix. By analyzing the XRD patterns in Fig. 6, the following results can be obtained:

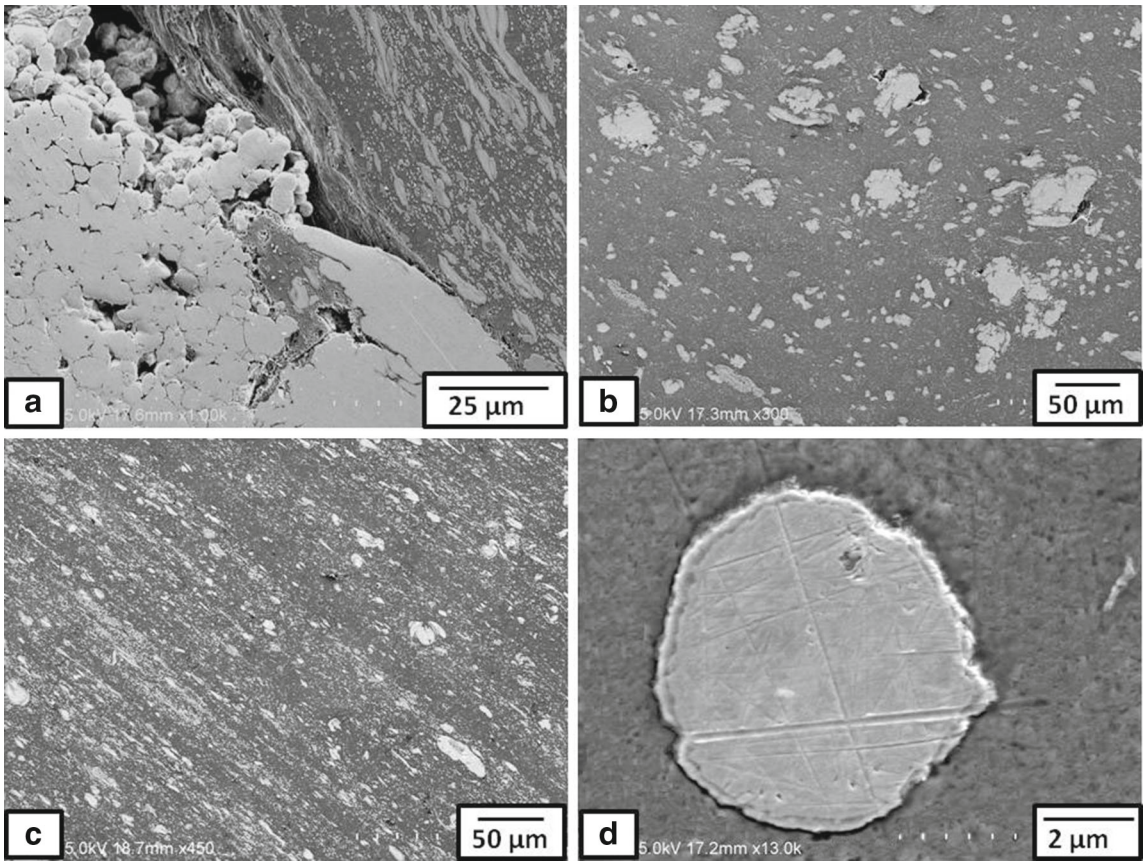

Fig. 4 SEM images of some local areas inside the nugget zones after first pass: **a** Cu clusters at 1500 rpm, **b** Cu particles distributions in the nugget zone center at 750 rpm, **c** banded structure at 750 rpm, and **d** higher magnification of Cu particle at 750 rpm

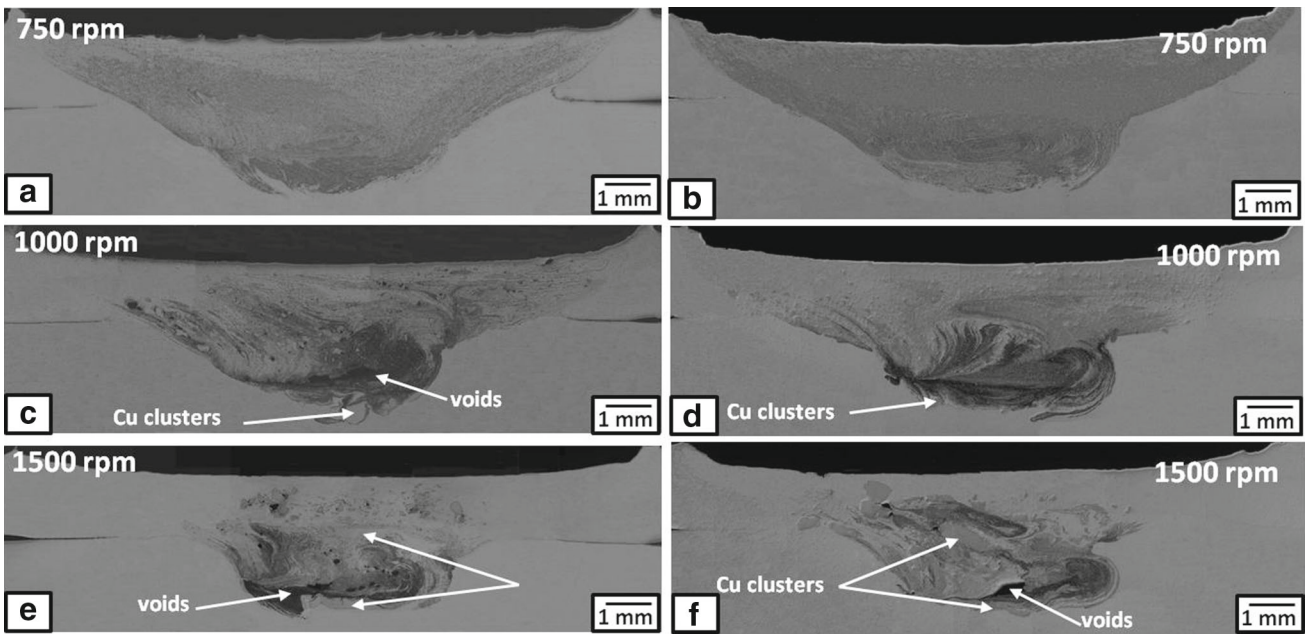

Fig. 5 Macrographs of the nugget zone cross section after triple FSP passes: **a**, **c** and **e** at traveling speed of 1.66 mm/s, while **b**, **d** and **f** at 0.83 mm/s

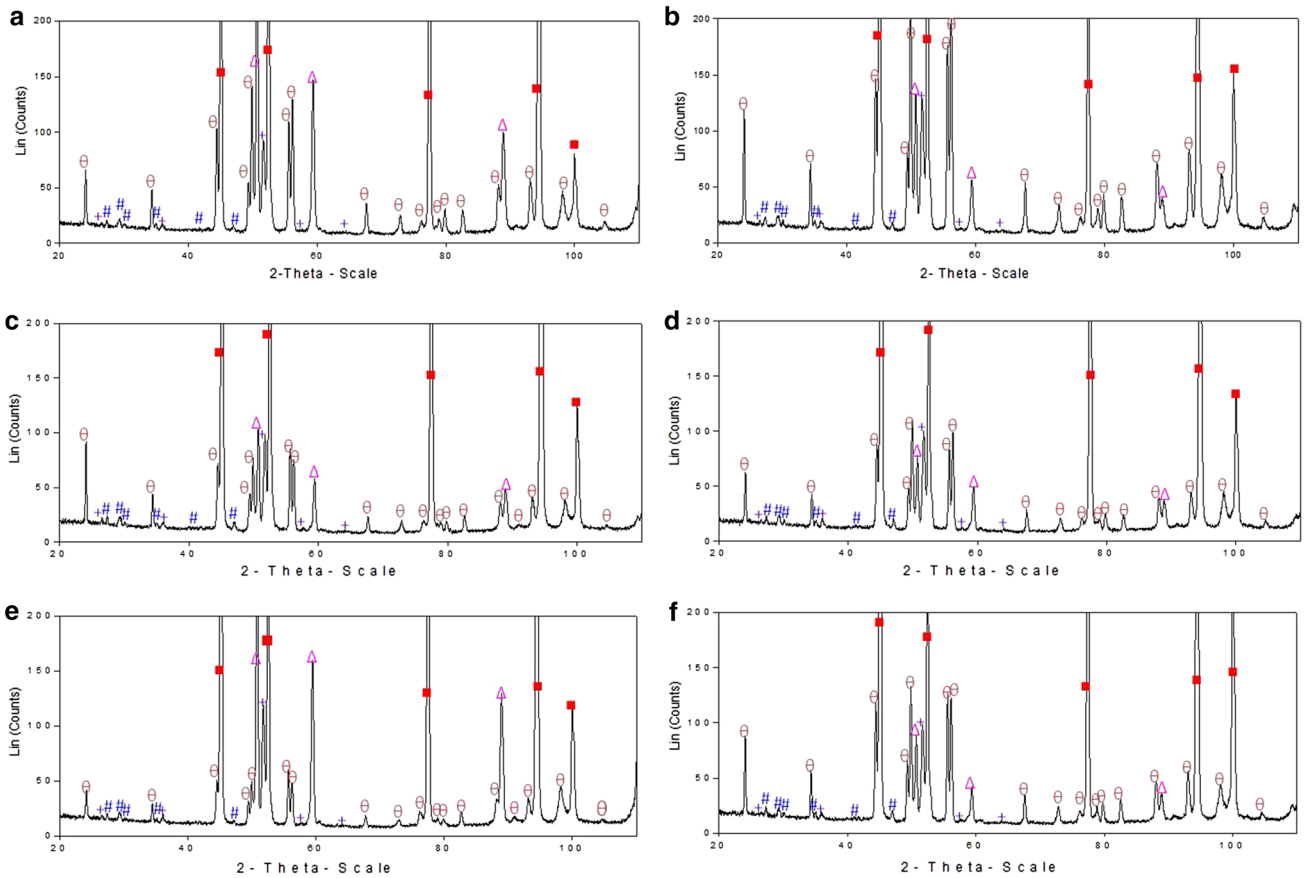

Fig. 6 XRD patterns obtained from the nugget zones cross sections after triple passes. (*filled square* Al, *triangle* Cu, *theta symbol* $CuAl_2$, *hash symbol* Al–Cu, *plus symbol* Al_4Cu_9). **a** 750 rpm and 1.66 mm/s. **b** 750 rpm and 0.83 mm/s. **c** 1000 rpm and 1.66 mm/s. **d** 1000 rpm and 0.83 mm/s. **e** 1500 rpm and 1.66 mm/s. **f** 1500 rpm and 0.83 mm/s

1. The diffraction peaks of the copper showed lower intensities than those observed after the first pass (compare Fig. 3 with Fig. 6), suggesting that the amount of non-reacted copper was decreased.
2. At a traveling speed of 1.66 mm/s, the peaks from the intermetallic phase $CuAl_2$ were higher at a rotation speed of 750 rpm, while the peaks from the Cu-rich phases (Al–Cu and Al_4Cu_9) were relatively higher at rotation speeds more than 750 rpm.
3. By decreasing the traveling speed from 1.66 to 0.83 mm/s, the Cu peaks were decreased at almost all rotation speeds. On the other hand, the intermetallic phase $CuAl_2$ showed the highest peaks at rotation speed of 750 rpm and a traveling speed of 0.83 mm/s.

The application of triple passes not only improves the homogeneity inside the nugget zone but also accelerates the reaction of the Cu particles with the Al matrix, since the heat generated in every pass promotes the diffusion and reaction. Moreover, application of multiple FSP passes enhances the separation of the Cu clusters/particles into isolated/smaller particles, as will be discussed later in this section, which also shares in the promotion of the reaction that forms the Al–Cu intermetallic compounds.

Although the $Cu/CuAl_2$ particles, as suggested in Fig. 7a, b, were distributed almost homogenously in the Al matrix at a tool rotation speed of 750 rpm, the un-reacted Cu content was considerably high at a traveling speed of 1.66 mm/s. This may be due to the lack of heat input during FSP at this tool rotation and traveling speeds for the copper particle of 5 μm diameter to react with the aluminum matrix. A magnified image of relatively larger dispersed Cu particle in the Al matrix, as shown in Fig. 7c, showed the formation of irregular-shape intermetallic compounds only on the edge of the particles, while the inner side of the particle remained as un-reacted copper as confirmed by the EDS analyses (at an acceleration voltage of 5 kV) in Fig. 7d, point 2. Moreover, the atomic concentrations of the Cu estimated from the EDS spectra at points 1 and 3 were about 29 and 70 %, respectively, suggesting the formation of $CuAl_2$ (point 1) and Al_4Cu_9 (point 3) intermetallic compounds. Also, based on the EDS analyses, most of the fine particles in Fig. 7a, b were identified as

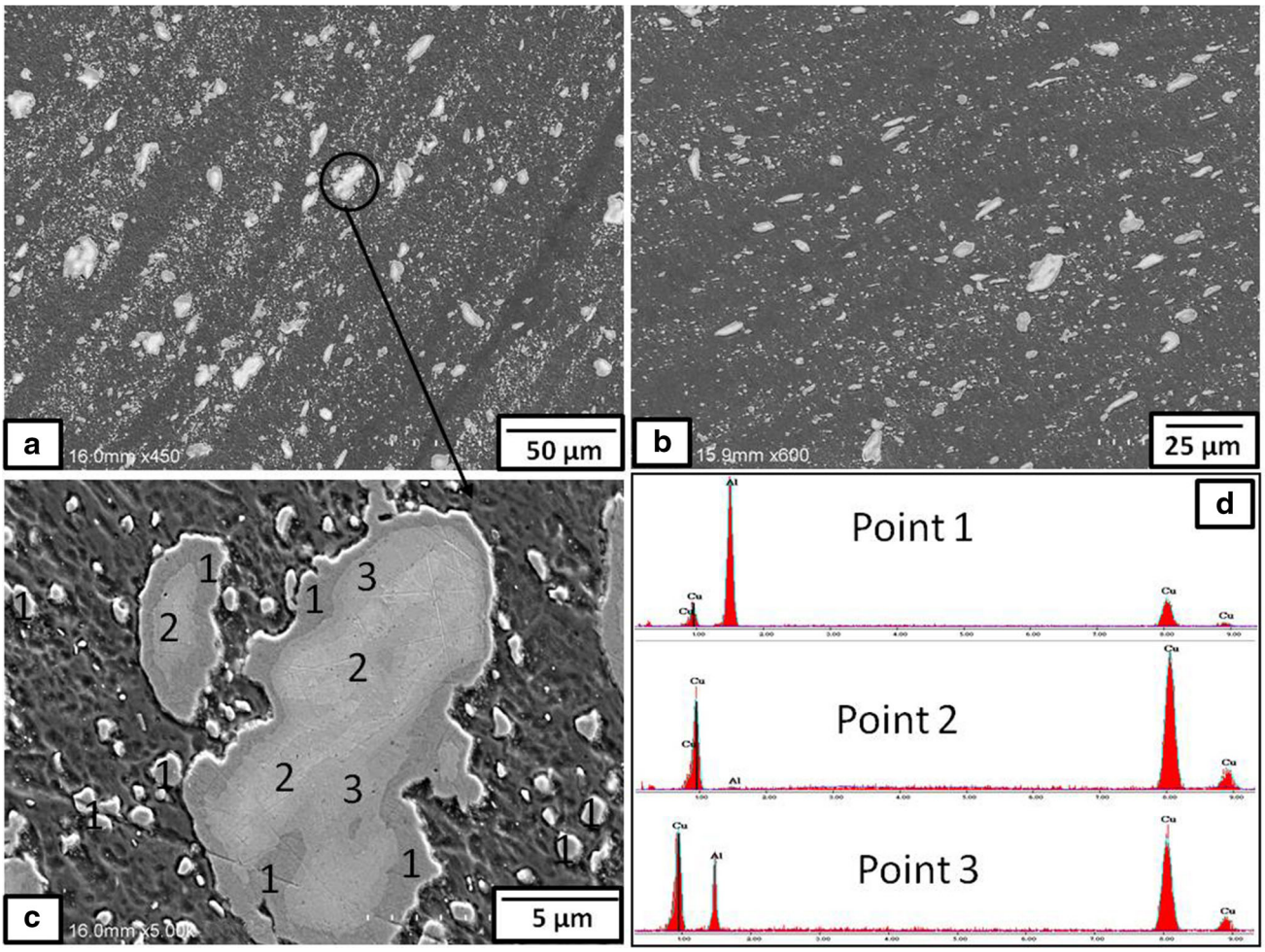

Fig. 7 SEM image of nugget zone fabricated by triple passes at a rotation speed of 750 rpm and a traveling speed of 1.66 mm/s: **a** advancing side, **b** retreating side, **c** enlarged image of selected area in **a** and **d** the EDS spectra from points 1, 2 and 3 in **c**

$CuAl_2$ intermetallics. In addition, these SEM images show the presence of very fine dispersed particles (less than 1 µm in size) and the average particle size of the dispersed particles in the nugget zone fabricated at rotation speed of 750 rpm was estimated to be about 2–3 µm, which was finer than the as-received Cu powder. This may be explained as a result of the stirring effect of the tool which can divide the particles into small parts.

By increasing the rotation speed to 1000 rpm, the Cu particles, as stated in Sect. 3.2.1, tended to be concentrated in the lower-center of the nugget zone, as shown in Fig. 8. Most of the Cu particles reacted with the Al matrix as shown in Fig. 8a, b, forming $CuAl_2$ intermetallics as suggested by the EDS spectrum shown in Fig. 8c. On the other hand, some unreacted Cu areas were detected at the bottom of the nugget zone as shown in Fig. 8d, e. The EDS spectra of some points in Fig. 8e give atomic content of the Cu of ~70 (points 1) and ~49 (points 2), which were the typical compositions of the Cu-rich intermetallics (Al–Cu and Al_4Cu_9) as shown in Fig. 8f.

When the rotation speed was increased to 1500 rpm, many bulk Cu areas were detected within the nugget zone, suggesting the occurrence of Cu particles consolidation prior to the reaction with the Al matrix, as shown in Fig. 9.

Based on these results, we may conclude that the lower rotation speed is beneficial for Cu and intermetallic particles distributions inside the nugget zone, whereas the heat generation necessary for the reaction between the Cu particles and the Al matrix is insufficient. On the other hand, the heat input obtained at high rotation speed is good for accelerating the reactions, but the Cu particles distributions within the nugget zone became inhomogeneous. Thus, it is preferable to use a low rotation speed for the homogeneity of particles distribution and increase the heat input by lowering the traveling speed for the enhancement of the reaction of Cu particles with aluminum matrix. As reported in many works [19–22], the maximum temperature during the FSW depends mainly on the rotation speed, while the period kept at high temperatures is a strong function of the traveling speed. Therefore, higher

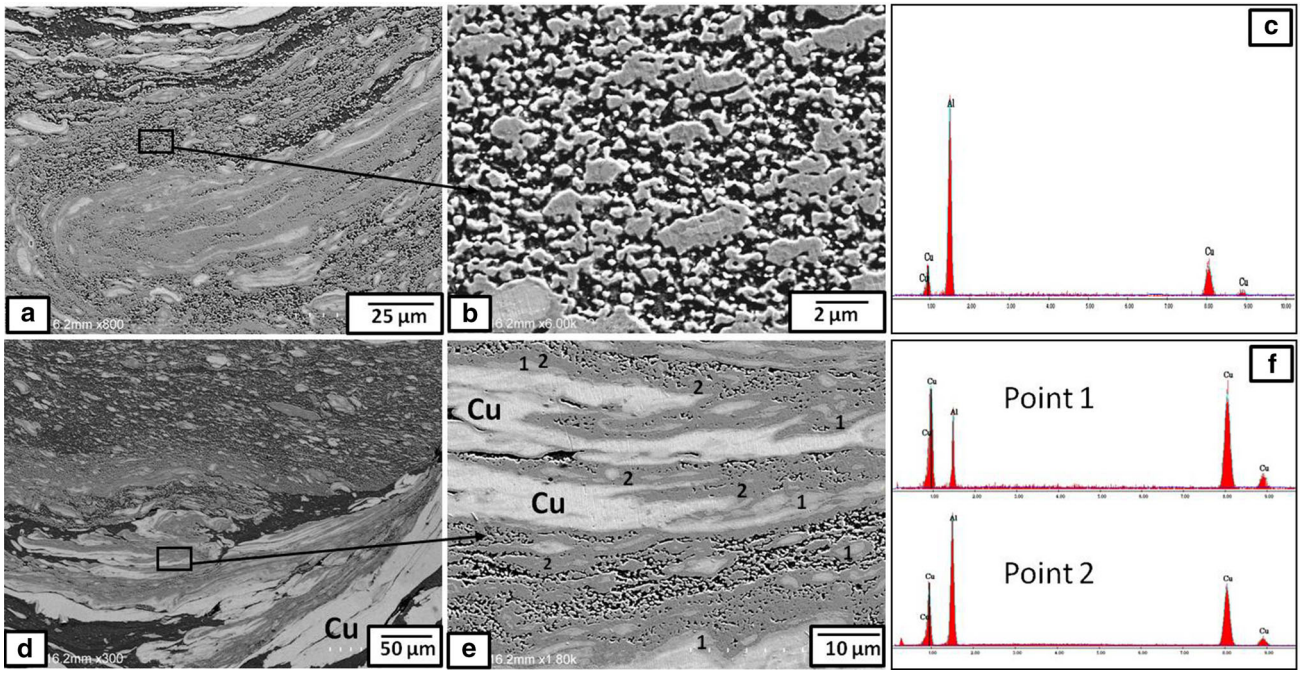

Fig. 8 SEM image of nugget zone fabricated with a rotation speed of 1000 rpm and a traveling speed of 1.66 mm/s after triple passes: **a** center, **b** enlarged image of selected area in **a**, **c** the EDS spectrum for all fine particles in **b**, **d** bottom side, **e** enlarged image of selected area in **d**, and **f** the EDS spectra for some points in **e**

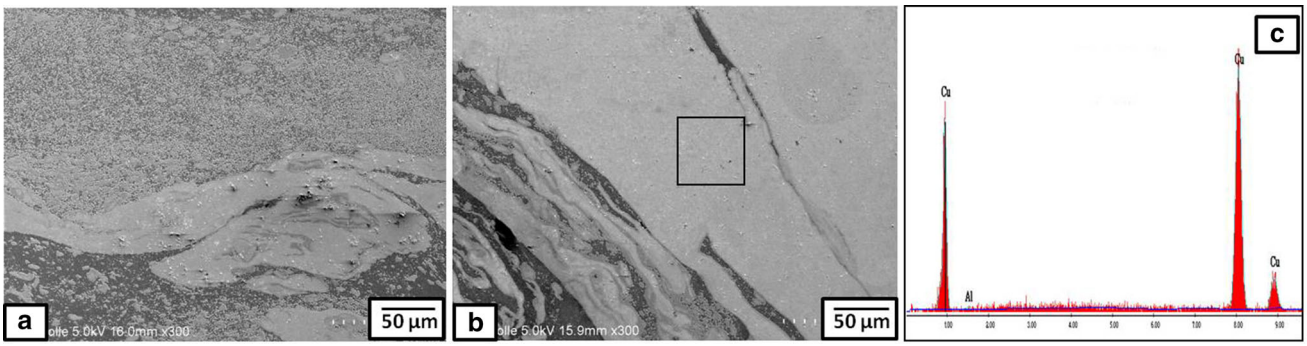

Fig. 9 SEM image of nugget zone fabricated by triple passes at a rotation speed of 1500 rpm and a traveling speed of 1.66 mm/s: **a** bottom, **b** Cu clusters and **c** the EDS spectrum obtained from the area indicated by the *square* in **b**

heat input is expected through decreasing the traveling speed to 0.83 mm/s.

The SEM microstructures observed in the nugget zone fabricated at a rotation speed of 750 rpm and a traveling speed of 0.83 mm/s are shown in Fig. 10. The particles are distributed almost uniformly in the matrix, and there were many fine particles less than 1 µm in size. The edges of relatively large dispersed particle, as shown in Fig. 10b, were irregular in shape, and there were very fine (nano-size) dispersed particles beside it (shown by arrows). The EDS analyses of these areas suggest that most of the large particles and all the fine particles were $CuAl_2$, while the inner parts were un-reacted copper phase as shown in Fig. 10c. A higher magnified image of the matrix area, as shown in Fig. 10d, indicated that many nano-sized intermetallics were dispersed in the aluminum matrix. These results suggests that the reaction products (mainly $CuAl_2$ intermetallics) were broken into very fine particles, removed from the Al/Cu particles interface by the stirring action of the FSP tool, and distributed in the matrix.

3.2.3 Hardness Measurements

The horizontal and vertical hardness profiles in the cross section of the nugget zone produced at a rotation speed of 750 rpm and traveling speed of 0.83 and 1.66 mm/s are presented in Fig. 11. The measurements were taken approximately at the middle of the cross section of the nugget

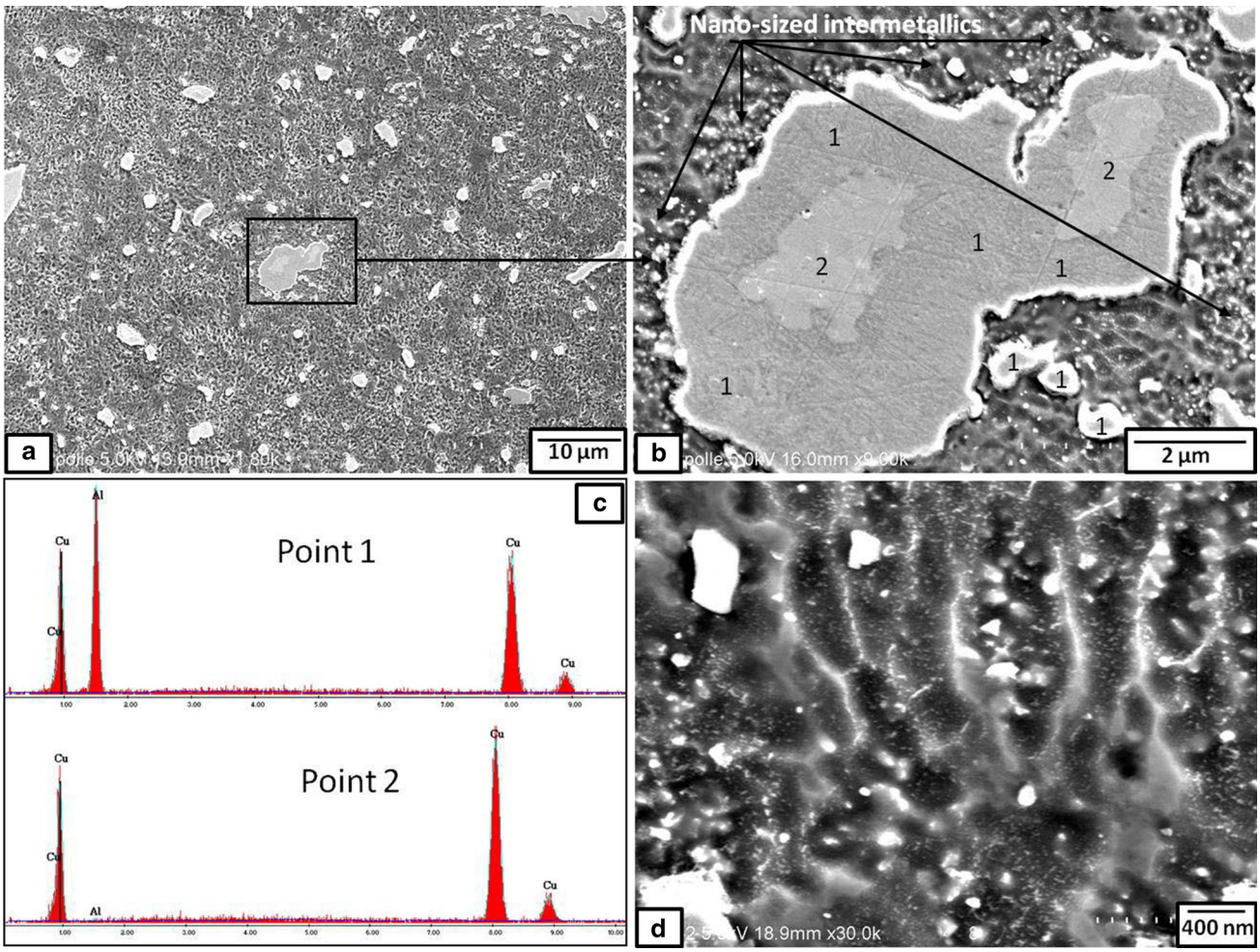

Fig. 10 SEM image of nugget zone fabricated at a rotation speed of 750 rpm and a traveling speed of 0.83 mm/s after triple passes: **a** nugget center, **b** enlarged image of selected area in **a**, **c** the EDS spectra for point 1 and 2 in **b**, and **d** matrix microstructure

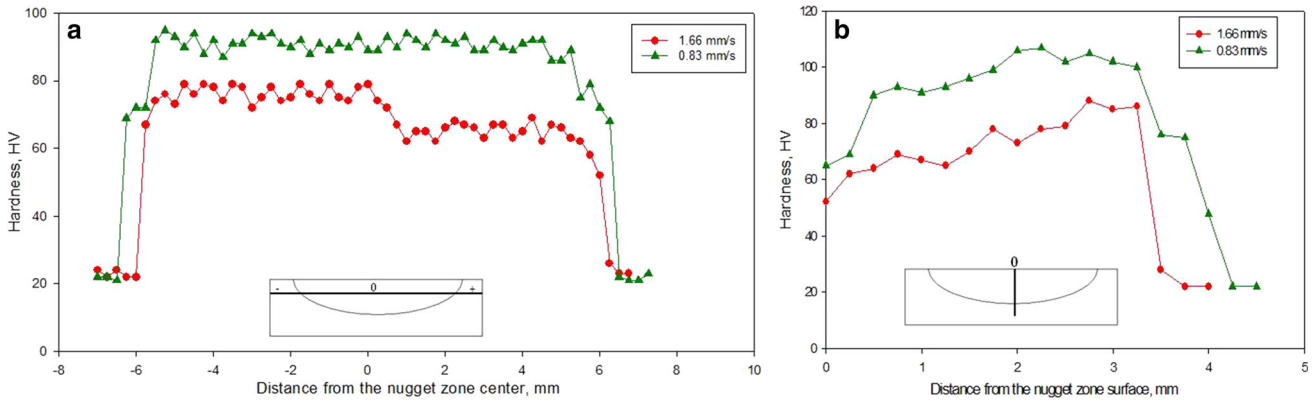

Fig. 11 Hardness distributions in **a** the horizontal and **b** vertical direction of the nugget zone fabricated with a rotation speed of 750 rpm and traveling speeds of 0.83 and 1.66 mm/s

as schematically shown in the insets at the lower part of the charts. Since the hardness profiles can be considered to reflect the homogeneity of the constituents of the nugget zone, the distributions of the hardness in the horizontal direction (Fig. 11a) suggests a reasonable homogeneity of the particles distribution in the nugget zone produced at a tool rotation speed of 750 rpm. The use of a traveling speed of 0.83 mm/s led to an increase in the average hardness to more

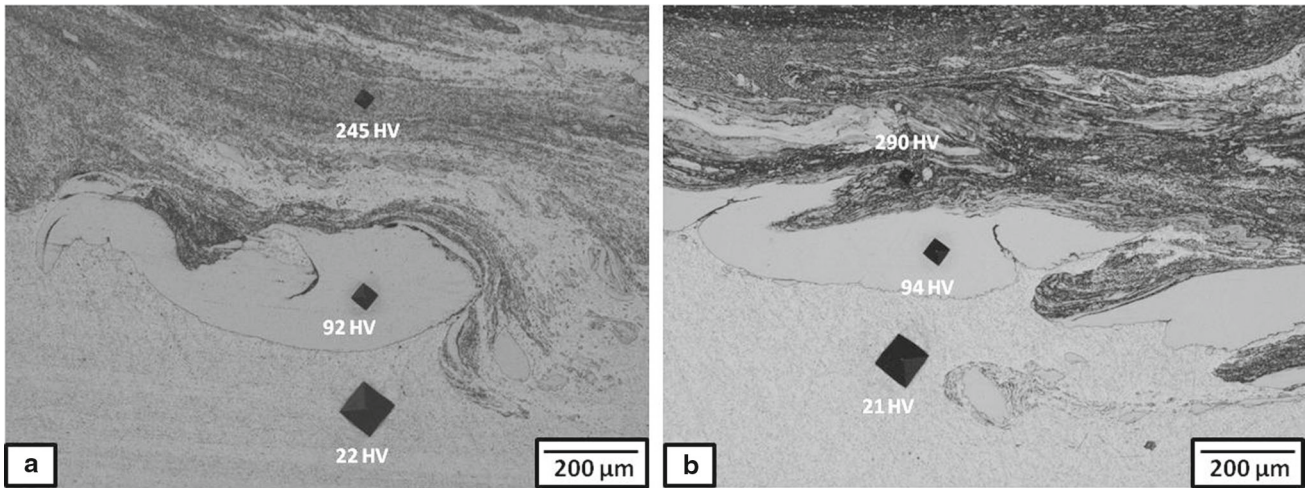

Fig. 12 Examples of the hardness indentations in the nugget zone fabricated at a rotation speed of 1500 rpm and traveling speeds: **a** 1.66 mm/s and **b** 0.83 mm/s

than 95 HV, which was almost five times as high as the hardness of the aluminum adjacent to the nugget zone. Regarding the hardness distribution in the vertical direction (Fig. 11b), the hardness values increased with the depth from the surface of the nugget zone at both traveling speeds, reaching ∼110 HV at the bottom of the nugget zone fabricated at a traveling speed of 0.83 mm/s.

When the rotation speed was more than 750 rpm, the hardness values shows great scattering inside the nugget zone. For example, at a rotation speed of 1500 rpm, as shown in Fig. 12a, the hardness values reached 245 HV in some areas of high intermetallic density, and it became about a 90 HV in the dense copper areas when the traveling speed was 1.66 mm/s. When the traveling speed was 0.83 mm/s, the hardness values reached 290 HV in places involving dense intermetallics, as illustrated in Fig. 12b.

3.2.4 Bending Tests

The macrographs of the nugget zones subjected to 90° face and side bending test are shown in Fig. 13, when the rotation speed was 750 rpm and the traveling speeds were 1.66 and 0.83 mm/s. When the traveling speed was 1.66 mm/s, the surface of the face bend test was sound without cracks or opening voids as shown in Fig. 13a. The nugget zone cross section, obtained of the same traveling speed of 1.66 mm/s, as shown in Fig. 13 b, was also sound on the side bending without cracks except some tearing in the upper portion of the heat-affected zone next to the nugget zone. This is may be due to the large difference in hardness and strength between the nugget zone and the heat-affected zone of the base metal.

When the traveling speed was decreased to 0.83 mm/s, small and large cracks were observed on the surface of the nugget zone after the face bending test, as shown in Fig. 13c. Some small cracks were also detected on the side-bending-tested surface almost in the same position as shown in Fig. 13d.

It was clear from these results that the ductility of the nugget zone fabricated at faster traveling speeds (1.66 mm/s) was higher than that fabricated at slower traveling speed (0.83 mm/s). This difference in ductility may be due to the microstructure of the matrix and due to the amount of intermetallic compounds formed during FSP.

4 Discussion

It is well known that friction stir processing (FSP) tool generates localized heating, severe plastic deformation and stirring of the constituents of the nugget zone. These generated heat and severe plastic strain can initiate the reaction of the Cu particles with the Al matrix, and the stirring action can accelerate it. Since the reaction between Cu and Al is exothermic, the heat accompanied by the reaction also contributes to the acceleration of the reaction [15–17]. On the other hand, the amount of the heat generated, temperature and processing time depends mainly on the tool design and processing parameters: rotation and traveling speeds.

Before proceeding into the details, it is better to mention the intermetallic phases in the Al–Cu system. According to the Al–Cu binary alloy phase diagram (Fig. 14, [23]), five intermetallics can be formed at temperatures above 380 ∘C: $CuAl_2$, CuAl, Cu_4Al_3, Cu_3Al_2 and Cu_9Al_4. The formation of any of these intermetallics in a place depends mainly on the Cu concentration and temperature in that place.

It is clear in this work that the lower rotation speeds improved the dispersed particles distributions inside the Al matrix and hence increased the surface areas of the Cu parti-

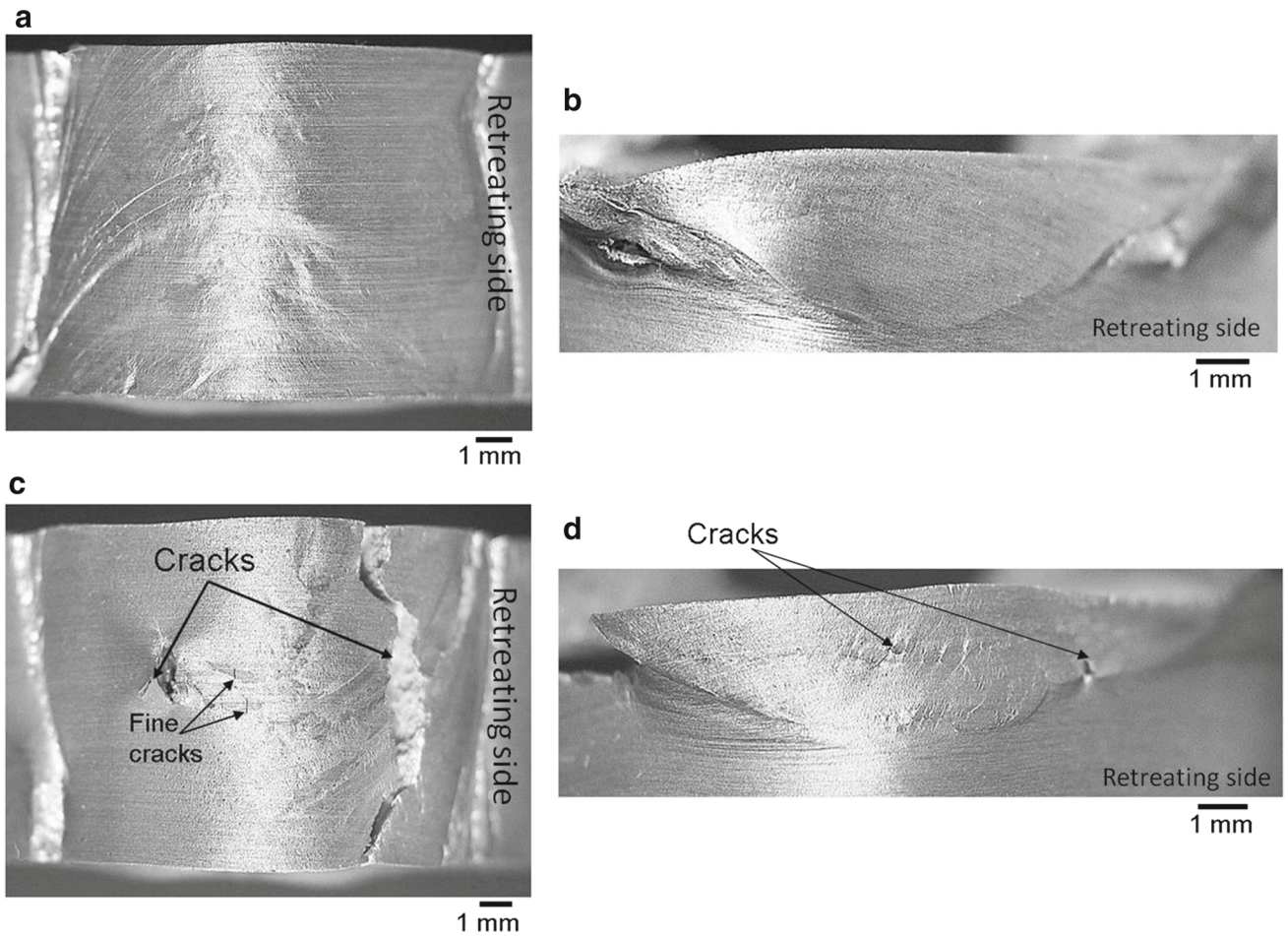

Fig. 13 Macrographs of the nugget zones after the bending tests on the specimens produced with triple FSP passes at a rotation speed of 750 rpm and traveling speed of 1.66 mm/s (**a** face bent, **b** side bent) and 0.83 mm/s (**c** face bent, **d** side bent)

cles that directly came into contact with the Al matrix, which promoted the reaction between them. At the same time, the decrease in the rotation speed was accompanied with relatively lowered heat generation in the nugget zone which was an essential factor for completing the reaction. On the other hand, increasing the rotation speed resulted in higher heat generation, but the dispersed particles were clustered in smaller areas in the nugget zone, which decreased the surface areas of the Cu particles that directly came in contact with the Al matrix. As mentioned in the Introduction section, our goal is to fabricate a layer where Al–Cu intermetallic particles are homogenously distributed. These contradictions in the merits of the rotation speed force the work toward the traveling speed. By using a minimum rotation speed of 750 rpm and half of the traveling speed (0.83 mm/s), the reactions between the Cu particles and the Al matrix were accelerated.

A characteristic feature that was observed in the nugget zone produced by dispersing the Cu particles was a dense distribution of the Al–Cu intermetallic compound particles much finer than the original size of the Cu particles (see Fig. 10). In relation to this, the Cu particles in the nugget zone presented very complicated morphologies quite different from those of the original spherical particle. These features suggest that the Cu particles were broken to form finer Al–Cu intermetallic compounds. It seems unlikely that the Cu particle itself was broken during the FSP, considering the excellent ductility of the copper. Possible mechanisms to explain these features are as follows:

1. Once the reaction between the Cu particles and the Al matrix was occurred, the reaction products (intermetallics), which are brittle, were fractured by the stirring action of the tool, and thrown away from the Cu particles, or
2. a localized liquation occurred in the boundary regions between the Cu particles and Al matrix from the heat generated by the FSP tool in addition to the heat generated by the reaction, because of the Al-$CuAl_2$ eutectic reaction at a temperature significantly lower than the melting point of the Al matrix, and the liquation region enriched in Cu was dispersed in the matrix by the stirring action. The intermetallic compound particles were formed from

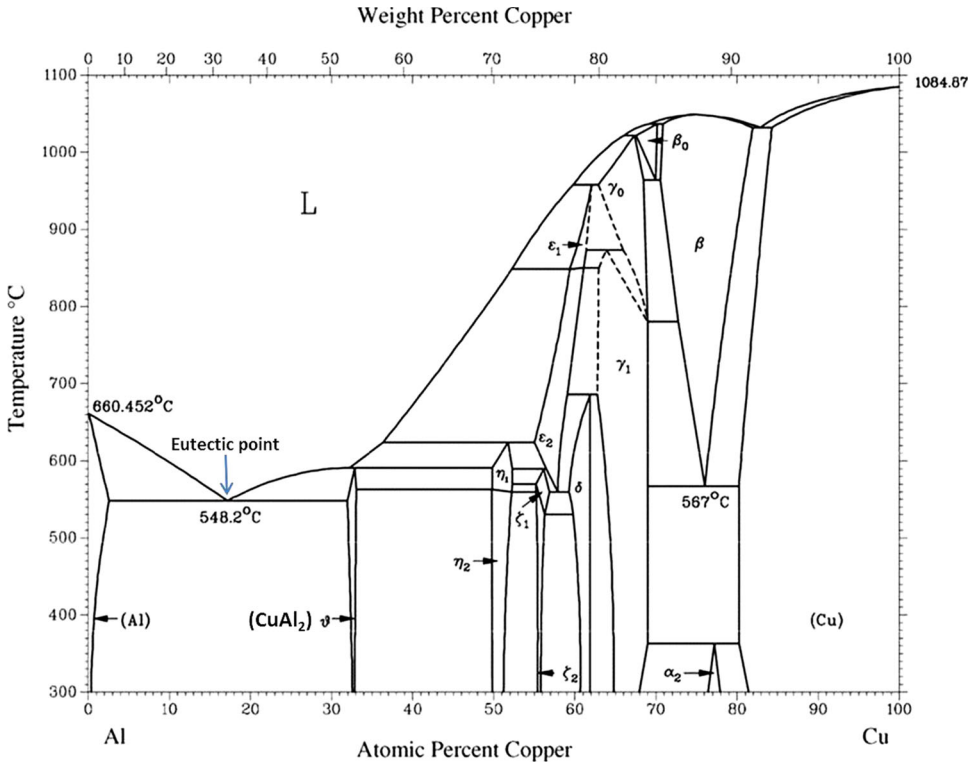

Fig. 14 Phase diagram of Cu–Al system [26]

these Cu-enriched liquation regions. In this case, the fine particles consist of only $CuAl_2$, and this is in accord with the experimental observation.

It is generally said that the FSW or FSP is a solid-state process. However, several authors have reported recently the occurrence of local or instantaneous liquation in the stir zone during the FSW [24–26].

Based on these results, the matrix consisted of very fine intermetallic compounds (mainly $CuAl_2$) which increase the hardness of the nugget zone to almost five times of the aluminum matrix adjacent to the nugget zone. This matrix structure reduces the nugget zone ductility to that it was cracked during bending test. Thus, the traveling speed of 1.66 mm/s was preferable if the ductility of the surface layer was desirable in any application.

5 Conclusions

In this work, a feasibility study has been carried out of the friction stir processing as a technique to fabricate a surface layer of Al–Cu intermetallic MMCs on aluminum surface. The Cu powder of 5 μm in size was packed in a groove of 3 mm width and 1.5 mm depth cut on the aluminum plate surface. The tool was rotated at a rate of 750–1500 rpm and traveled at speeds of 0.83 and 1.66 mm/s. Double and triple passes were applied. The results obtained can be summarized as follows:

1. The copper particles reacted with the aluminum matrix at almost all the processing conditions even during the first pass.
2. At a traveling speed of 1.66 mm/s, most of the resulted intermetallics were $CuAl_2$ at a rotation speed of 750 rpm, while the Cu-rich intermetallics (Al–Cu and Al_4Cu_9) appeared at rotation speeds of 1000 and 1500 rpm.
3. When the traveling speed was decreased to 0.83 mm/s, the amounts of the resulted intermetallics were increased.
4. At a rotation and traveling speeds of 750 rpm and 0.83 mm/s, respectively, the nugget zone matrix consisted of nano-sized $CuAl_2$ intermetallics distributed in aluminum which increase the hardness to almost five times of the aluminum matrix adjacent to the nugget zone.
5. The ductility of the nugget zone fabricated at a traveling speed of 1.66 mm/s was higher than that fabricated at 0.83 mm/s, when the rotation speed was 750 rpm.

References

1. Mishra, R.S.; Ma, Z.Y.: Friction stir welding and processing. Mater. Sci. Eng. R **50**, 1–78 (2005)

2. Rajesh, S.; Gopala, K.A.; Rama, M.R.P.; Duraiselvam, M.: Statistical analysis of dry sliding wear behavior of graphite reinforced aluminum MMCs. Proc. Mater. Sci. **6**, 1110–1120 (2014)
3. de Portu, G.; Guicciardi, S.; Melandri, C.; Monteverde, F.: Wear behaviour of Al_2O_3–Mo and Al_2O_3–Nb composites. Wear **262**, 1346–1352 (2007)
4. Fu, H.; Han, K.; Song, J.: Wear properties of Saffil/Al/Al_2O_3/Al and Saffil/SiC/Al hydrid metal matrix composites. Wear **256**, 705–713 (2004)
5. Dubourg, L.; Hiawka, F.; Cornet, A.: Study of aluminium–copper–iron alloys: application for laser cladding. Surf. Coat. Technol. **151**(152), 329–332 (2002)
6. Bhrigu, A.; Michael, K.; Konstantin, Y.N.; Michael, S.: Fabrication and characterization of high strength Al–Cu alloys processed using laser beam melting in metal powder bed. Phys. Proc. **56**, 135–146 (2014)
7. Zhang, Z.; Han, B.Q.; Witkin, D.; Ajdelsztajn, L.; Laverna, E.J.: Synthesis of nanocrystalline aluminum matrix composites reinforced with in-situ devitrified Al–Ni–La amorphous particles. Scr. Mater. **54**, 869–874 (2006)
8. Feng, J.C.; Cao, J.; Li, Z.R.: Microstructure evolution and reaction mechanism during reactive joining of TiAl intermetallic to TiC cermet using Ti–Al–C–Ni interlayer. J. Alloys Compd. **436**, 298–302 (2007)
9. Roy, D.; Ghosh, S.; Basumallick, A.; Basu, B.: Preparation of Fe-aluminide reinforced in situ metal matrix composites by reactive hot pressing. Mater. Sci. Eng. A **415**, 202–206 (2006)
10. Krasnowski, M.; Kulik, T.: Nanocrystalline FeAl intermetallic produced by mechanical alloying followed by hot-pressing consolidation. Intermetallics **15**, 201–205 (2007)
11. Sexton, L.; Lavin, S.; Byrne, G.; Kennedy, A.: Laser cladding of aerospace materials. J. Mater. Process. Technol. **122**, 63–68 (2002)
12. Znamirowski, Z.; Pawlowski, L.; Cichy, T.; Czarczynski, W.: Low macroscopic field electron emission from surface of plasma sprayed and laser engraved TiO_2, Al_2O_3+13TiO_2 and Al_2O_3+40TiO_2 coatings. Surf. Coat. Technol. **187**, 37–46 (2004)
13. Omar, S.; Salih, H.O.; Sun, W.; McCartney, D.G.: A review of friction stir welding of aluminium matrix composites. Mater. Des. **86**(5), 61–71 (2015)
14. Uyyuru, R.K.; Surappa, M.K.; Brusethaug, S.: Effect of reinforcement under dry sliding conditions. Tribol. Int. **40**(2), 365–373 (2007)
15. Mishra, R.S.; Mahoney, M.W.; McFadden, S.X.; Mara, N.A.; Mukherjee, A.K.: High strain rate superplasticity in a friction stir processed 7075 Al alloy. Scr. Mater. **42**, 163–168 (2000)
16. Mishra, R.S.; Ma, Z.Y.; Charit, I.: Friction stir processing: a novel technique for fabrication of surface composite. Mater. Sci. Eng. A. **341**, 307–310 (2003)
17. Raju, L.S.; Kumar, A.: Influence of Al_2O_3 particles on the microstructure and mechanical properties of copper surface composites fabricated by friction stir processing. Def. Technol. **10**(4), 375–383 (2014)
18. Hsu, C.J.; Chang, C.Y.; Kao, P.W.; Ho, N.J.; Chang, C.P.: Al–Al_3Ti nanocomposites produced in situ by friction stir processing. Acta Mater. **54**, 5241–5249 (2006)
19. Hsu, C.J.; Kao, P.W.; Ho, N.J.: Intermetallic-reinforced aluminum matrix composites produced in situ by friction stir processing. Mater. Lett. **61**, 1315–1318 (2007)
20. Hsu, C.J.; Kao, P.W.; Ho, N.J.: Ultrafine-grained Al-Al_2Cu composite produced in-situ by friction stir processing. Scr. Mater. **53**, 341–345 (2005)
21. Lee, I.S.; Kao, P.W.; Ho, N.J.: Microstructure and mechanical properties of Al–Fe in situ nanocomposite produced by friction stir processing. Intermetallics **16**, 1104–1108 (2008)
22. Arbegast, W.J.; Hartley, P.J.: Proceedings of the 5th International Conference on Trends in Welding Research, June 1–5, p. 541, Pine Mountain, GA (1998)
23. Arbegast, W.J.; Hartley, P.J.: Alloy Phase Diagram, ASM Metals Handbook, vol. 3. ASM International, Ohio (1992)
24. Sato, Y.S.; Park, S.H.C.; Michiuchi, M.; Kokawa, H.: Constitutional liquation during dissimilar friction stir welding of Al and Mg alloys. Scr. Mater. **50**, 1233–1236 (2004)
25. Feng, Z.H.; Ma, Z.Y.: Formation of Cu_2FeAl_7 phase in friction-stir-welded SiCp/Al–Cu–Mg composite. Scr. Mater. **57**, 1113–1116 (2007)
26. Mohammadi, J.; Behnamian, Y.; Mostafaei, A.; Gerlich, A.P.: Tool geometry, rotation and travel speeds effects on the properties of dissimilar magnesium/aluminum friction stir welded lap joints. Mater. Des. **75**(15), 95–112 (2015)